

Design and Implementation of Terahertz Near-Field Imaging Of Dielectric Resonators

1. SAPAVAT DEEPA

ABSTRACT:

As an alternative to metallic resonators, dielectric resonators can increase radiation efficiencies of metasurfaces at terahertz frequencies. Such subwavelength resonators made from low-loss dielectric materials operate on the basis of oscillating displacement currents. For full control of electromagnetic waves, it is essential that dielectric resonators operate around their resonant modes. Thus, understanding the nature of these resonances is crucial towards design implementation. To this end, an array of silicon resonators on a quartz substrate is designed to operate in transmission at terahertz frequencies. The resonator dimensions are tailored to observe their low-order modes of resonance at 0.58 THz and 0.61 THz respectively. We employ a terahertz near-field imaging technique to measure the complex near-fields of this dielectric resonator array. This unique method allows direct experimental observation of the first two fundamental resonances.

1. INTRODUCTION

Metasurfaces or two-dimensional metamaterials [1] consist of miniaturized resonators with subwavelength periodicity, and are capable of manipulating the wavefront of incident waves. The principle of metasurfaces to control the wavefront reconciles with that of reflectarrays [2] and transmitarrays [3], well established at microwave frequencies. Conventionally, metallic resonators are employed for shaping wavefronts either through reflection [2, 4] or transmission by using multilayer configurations [5,6]. Typically, metallic resonators exhibit decreasing radiation

efficiencies with increasing frequencies. This is due to increasing Ohmic loss at frequencies beyond the microwave regime [7]. In contrast, metasurfaces made of dielectric resonators have been shown to intrinsically maintain high efficiencies from the microwave to the visible frequency range [8, 9]. As dielectric resonators operate based on the oscillation of displacement current at specific resonance frequencies, Ohmic loss is alleviated, and dielectric losses can be minimized through the use of low-loss dielectric materials [10]. Apart from the superior efficiency as discussed above, dielectric resonators can support magnetic dipole resonances with a single

dielectric layer, as opposed to two layers required by their metal counterparts. With proper magnetic and electric resonances, dielectric resonator metasurfaces can exhibit extraordinary phase, amplitude and polarization control of output waves. As for the phase control, individual resonators can induce a phase discontinuity within the 2π range for shaping the outgoing wavefront in transmission [11–13] and reflection [8, 9, 14]. A number of components have exploited electric and magnetic resonances in dielectric resonators for different functions, which include generation of holograms [15] and optical vortices [16]. Other research works have demonstrated ways to mechanically tune dielectric resonator arrays as crucial steps towards implementing high performance reconfigurability [17, 18]. In the terahertz frequency regime, high-efficiency components are particularly important as power is generally limited and there is degradation in the signal-to-noise ratio due to free-space path loss and atmospheric absorption. Practical applications for terahertz metasurfaces of subwavelength metallic resonators have been proposed in sensing [19–22], filtering [23] and wavefront manipulation [24–28]. Dielectric resonators have the potential to become

crucial building blocks in the terahertz frequency region by increasing the efficiency of basic components. Magnetic mirrors and reflectarrays based on dielectric resonators that exploit the properties of magnetic resonances have been realized with high performance [29, 30]. Terahertz dielectric resonators that utilize overlapping magnetic and electric resonances have been designed and experimentally validated. Some applications include extraordinary wavefront manipulation in reflection [31] and a highly efficient absorber [32]. Currently, most metasurfaces are characterized by far-field measurements using terahertz time-domain spectroscopy systems (THz-TDS). However, terahertz far-field measurements are lacking the microscopic resolution needed to investigate the properties of samples in the near-field. Importantly, reactive near-fields cannot be observed through far-field measurement. In contrast, terahertz near-field microscopy has been useful in mapping the two-dimensional electromagnetic responses of various samples with spatial resolutions below the diffraction limit [33–35]. Some components characterized by terahertz near-field microscopy include metallic resonators [36–38], metallic subwavelength holes [39] and dielectric microspheres made of Vol. 25,

No. 4 | 20 Feb 2017 | OPTICS EXPRESS
3758 high-permittivity TiO₂ ($\epsilon_r \approx 100$) [40]. Here, we conduct a near-field measurement to examine the properties of the fundamental electric and magnetic dipole resonances of a dielectric resonator array, fabricated via a top-down approach. Understanding these fundamental resonances is essential towards designing highly efficient metasurfaces.

2. DESIGN OF TERAHERTZ DIELECTRIC RESONATORS

A terahertz dielectric resonator array is constructed from periodically arranged silicon cylinders on a quartz substrate. The cylindrical shape of the resonator is chosen mainly because of its isotropy. Furthermore, periodically arranged cylindrically shaped resonators are worth investigating due to their practicality for planar integration and robustness in design implementation, particularly for wave manipulation with metasurfaces. In addition, inter-resonator coupling that exists within arrays cannot be observed in an individual resonator. The operation of dielectric resonators can be described by their quality factors: This includes Q_{rad}, which is inversely proportional to radiation loss, and Q_d which is inversely proportional to energy loss to dissipation in the materials. It is not advisable to have high Q_{rad} as a sharp

resonance only allows for narrowband operation of metasurfaces. For potential applications in wave manipulation over a relatively large bandwidth, it is ideal that the dielectric resonator exhibits a high Q_d and moderate Q_{rad}. Thus, high-resistivity float-zone silicon is chosen as the dielectric material as it has moderate relative permittivity $\epsilon_r = 11.68$ and negligible loss [41]. The substrate is quartz with thickness of 500 μm and relative permittivity $\epsilon_r = 3.8$ with loss tangent $\tan \delta = 0.01$ [42]. The structure has high Q_d as low-loss dielectrics have been utilized in the design and moderate Q_{rad} as the resonator has a moderate effective permittivity. As our quartz substrate is more than one wavelength thick, it contributes to the resonance properties of our dielectric resonator array. The resonator height of 82 μm and the radius of 105 μm are selected to exhibit electric and magnetic dipole resonances centered around 0.60 THz. The unit cell of the dielectric resonator array is 245 μm which is explicitly chosen to be less than half the operating wavelength ($\lambda = 500 \mu\text{m}$) to avoid diffraction. Numerical computations are performed by using the frequencydomain solver in CST Microwave Studio. The periodic boundary conditions are applied to the unit cell to replicate an

infinite uniform array of the resonators. The fundamental modes of resonance excited in this dielectric resonator array are the $TM_{01\delta}$ for the electric dipole resonance and the $HEM_{11\delta}$ for the magnetic dipole resonance [10]. We can classify the electric and magnetic dipole resonance modes by examining their electric and magnetic fields, as revealed by cross-sectional views in Fig. 1. The electric dipole resonance (Fig. 1a) shows an electric field that is oscillating in the direction of the incident wave's polarization (E_y). Magnetic dipole resonances (Fig. 1b) can be identified with a circulating electric field around the center of the resonator. The symmetry of the periodic array in the xy -plane induces symmetric mutual coupling, and thus the field distribution shows the corresponding symmetry, in the y -direction. Due to the presence of a substrate in the dielectric

resonator array, free-space illumination from the $+z$ direction causes asymmetry of the field distribution in the z -direction.

3. FABRICATION For this structure, micro-fabrication approach involves a combination of SU-8 assisted bonding, photolithography, and deep reactive ion etching (DRIE). To begin with, a thin adhesion layer of SU-8 is spin-coated on a 3-inch quartz wafer. A 125 μm thick, high-resistivity silicon wafer is then bonded to the substrate by passing it through a laminator at 100 $^\circ\text{C}$ at slow speed. The bonded silicon is thinned down as per the design requirements by plasma-enhanced DRIE (Oxford PlasmaPro 100 Estrelas). Finally, the silicon layer is patterned with thick photoresist (AZ4562) and subsequently etched down with the Bosch silicon etching process to realize an

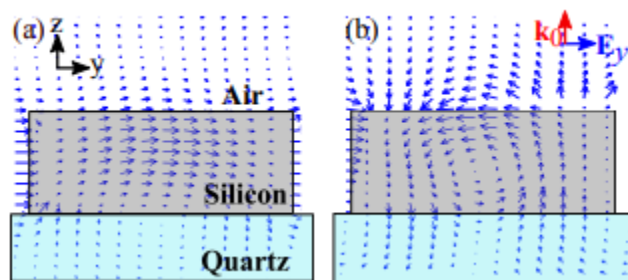


Fig. 1. Cross-sectional view of a single dielectric resonator. The instantaneous electric fields are represented by blue

arrows. (a) Electric dipole resonance and (b) magnetic dipole resonance. The wave is

incident from the substrate side, and it is polarized in the y-direction.

array of cylinders. It should be noted that, considering the low thermal conductivity of quartz, the aforementioned etching steps are performed at -5°C . Fabricated structures are imaged using scanning electron microscopy

(FEI Verios SEM). False-color and optical profiler images of the fabricated dielectric resonator array are shown in Fig. 2 and in Fig. 3 respectively. These images are representative of the impeccable quality and high detail accuracy of the fabricated samples.

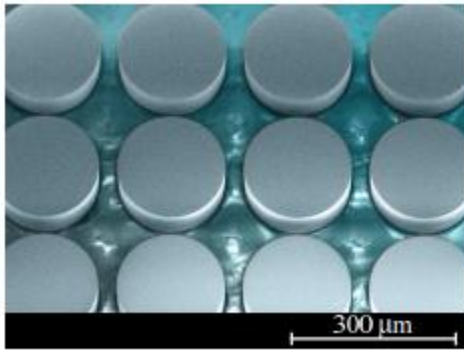


Fig. 2. Scanning electron micrograph of the fabricated silicon resonators.

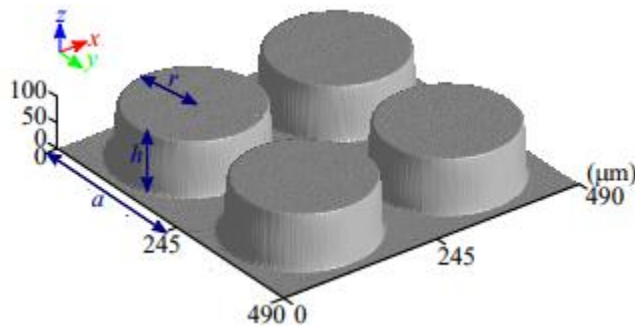


Fig. 3. Optical profiler image of the fabricated silicon resonators. The dimensions are as follows: the unit cell size $a = 245\ \mu\text{m}$, the resonator height $h = 82\ \mu\text{m}$, and the resonator radius $r = 105\ \mu\text{m}$.

4. MEASUREMENTS AND RESULTS

4.1. FAR-FIELD ANALYSIS AND RESULTS A standard THz-TDS system is used for far-field measurements. A focused beam with a spot size of 5 mm illuminates the sample from the substrate side to excite approximately 300 dielectric resonators. A blank quartz substrate of the same thickness ($500\ \mu\text{m}$) is used as a reference. All the

measurements are conducted in a nitrogen-purged atmosphere to mitigate the water vapour absorption. Fourier transform is applied to the time-resolved data to obtain the complex frequency response of the sample with a spectral resolution of 5 GHz. The transmission amplitude is shown in Fig. 4. From the normalized spectrum, we can observe the dips at 0.58 THz and 0.61 THz which correspond to the electric dipole resonance and magnetic dipole resonance respectively. The strength and position of these resonances differ slightly from the results obtained from numerical simulation with CST Microwave Studio. This could be due to the realized focused beam as opposed to numerical plane-wave approximation [43]. A relatively large resonance width can be observed in Fig. 4 which corresponds to a moderate Qrad factor, as designed. Based on theoretical calculations in [10], we would expect a lower Qrad factor for a magnetic dipole resonance ($Q_{rad} = 9.15$) as compared to an electric dipole resonance ($Q_{rad} = 9.43$). This is because the field distribution of the magnetic dipole resonance is less confined within the dielectric resonator resulting in a slightly lower radiative Q factor as compared to the electric dipole resonance. Apart from that, higher-order modes can also be observed at higher

frequencies in both the simulation and measurement.

4.2. NEAR-FIELD SETUP AND ANALYSIS

As shown in Fig. 5, the near-field experiment setup is based on a typical THz-TDS system, with the major difference being that the electro-optic crystal is placed very close to the sample to collect reactive fields emerging from the sample. In order to measure the longitudinal electric fields, E_z , we used an electro-optic crystal in the (100) orientation. The dielectric resonator array is illuminated from the back of the substrate with a y-polarized focused Gaussian beam with a spot diameter of 500 μm . The E_z field measurement is taken at approximately 100 μm ($\lambda/5$) above the dielectric resonator array to minimize electric field disturbance. It is also possible to measure the transverse components, E_x and E_y using electro-optic crystals of the (110) orientation [44]. However, measurements of the transverse components (E_x and E_y) are not utilized in this work, since local evanescent transverse components outside the dielectric resonators are relatively weak. This weak field is obscured by the propagating terahertz waves that co-propagate with the probe beam throughout the crystal length. It is noteworthy that in metallic subwavelength

apertures [45] and planar metamaterials [37], it is possible to

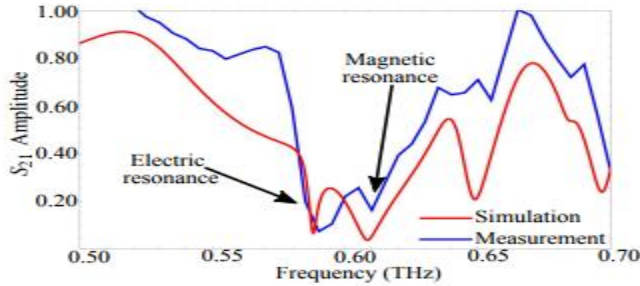


Fig. 4. Normalized transmission spectra of the dielectric resonator array

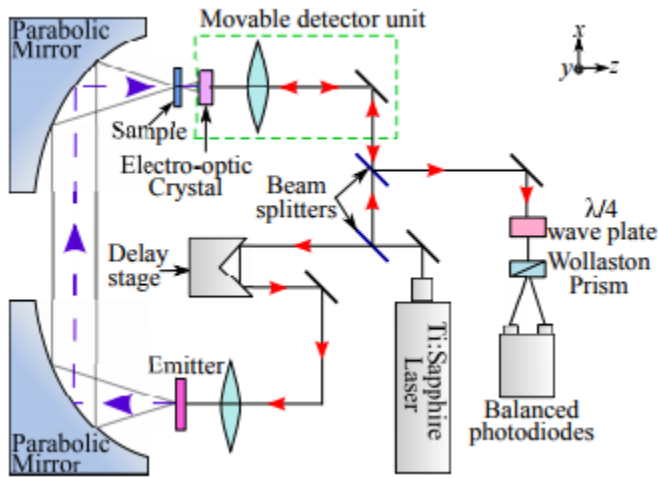


Fig. 5. Near-field THz-TDS experimental set up. The purple arrows represent the THz pulses and the red arrows indicate the infrared laser beam paths.

measure all three components of the electric field, owing to their exposed strong localized field. The employed near-field system can measure the electric field in one spot at a time with a spot diameter of $10 \mu\text{m}$ which is defined by the probe laser. A 2D raster scan is performed by moving the electro-optic crystal together with the laser

beam with translation stages. The longitudinal (z-directed) electric fields hence is mapped over the xy plane with a spatial resolution of $20 \mu\text{m}$. A complete set of measurements for each near-field spot consists of a total electric field measurement of the E_z component, $E_{z,t}(t)$, in the presence of the sample, and a reference or incident electric field measurement $E_{z,r}(t)$, measured with a bare quartz substrate replacing the sample. To obtain the scattered electric field, $E_{z,s}(t)$, which is the electric

field due to interaction with the resonator solely, we subtract the reference electric field from the total electric field in the frequency domain. From data analysis a slight temporal shift is observed between the reference and sample measurements. To mitigate the effect of this shift, a phase offset ($\Delta\phi$) can be added to the reference measurement: A slight spatial misalignment of the measured results is also observed in the xy dimensions. This can be straightforwardly compensated by shifting the alignment between the sample and reference data.

4.3. NEAR-FIELD RESULTS As a comparison, we simulate the dielectric resonator array with CST Microwave Studio, with a 100 μm air gap space between electro-optic crystal ($\epsilon_r = 2.25$) and sample to match experimental conditions. The measured and simulated instantaneous electric fields for both electric and magnetic dipole resonances are shown in Fig. 6. The fields are at the moment when the oscillation reaches their maximum amplitude and are also normalized to the maximum amplitude of the electric fields for the simulated magnetic dipole resonance. The measured near-field images show horizontal variations in amplitude which are due to the focused beam used during measurement. From the

simulations, we can observe that the Ez field for the magnetic resonance is stronger than the electric resonance. As both simulated and measured plots are normalized to the same scale, the same observation is confirmed in the measured results. This relatively strong Ez field is due to the out-of-the-plane circulation of the electric field for the magnetic resonance.

CONCLUSION In conclusion, we have designed and experimentally validated an array of terahertz dielectric resonators operating in transmission at terahertz frequencies. As the resonant electric fields are mostly confined within the dielectric resonators themselves, these fields are not readily accessible via near-field probe. This is in contrast to metallic resonators where resonant electric fields are not confined within the structure facilitating access to near-field transverse electric field components. Nevertheless, we have investigated dielectric resonator structures with both far-field spectroscopy and near-field spectroscopy. We achieved good agreement between our measured and simulated results for both the far-field and near-field measurements. With near-field THz-TDS techniques, we confirm the presence of the predicted fundamental electric resonance mode at 0.58 THz and the

magnetic resonance mode at 0.61 THz. Electromagnetic interactions between the resonators observed in the near-field provides information that cannot be obtained in the far-field which is useful for potential future applications of metasurfaces.

REFERENCES AND LINKS

1. N. I. Zheludev and Y. S. Kivshar, “From metamaterials to metadevices,” *Nat. Mater.* 11, 917–924 (2012).
2. J. Huang and J. A. Encinar, *Reflectarray Antennas*, vol. 30 (John Wiley & Sons, 2007).
3. C. G. Ryan, M. R. Chaharmir, J. Shaker, J. R. Bray, Y. M. Antar, and A. Ittipiboon, “A wideband transmitarray using dual-resonant double square rings,” *IEEE Trans. Antennas Propag.* 58, 1486–1493 (2010).
4. N. Yu, P. Genevet, M. A. Kats, F. Aieta, J.-P. Tetienne, F. Capasso, and Z. Gaburro, “Light propagation with phase discontinuities: generalized laws of reflection and refraction,” *Science* 334, 333–337 (2011).
5. C. Pfeiffer, N. K. Emani, A. M. Shaltout, A. Boltasseva, V. M. Shalaev, and A. Grbic, “Efficient light bending with isotropic metamaterial Huygens’ surfaces,” *Nano Lett.* 14, 2491–2497 (2014).
6. C. Pfeiffer and A. Grbic, “Cascaded metasurfaces for complete phase and polarization control,” *Appl. Phys. Lett.* 102, 231116 (2013).
7. J. B. Khurgin, “How to deal with the loss in plasmonics and metamaterials,” *Nature* 10, 2–6 (2015).
8. L. Zou, W. Withayachumnankul, C. M. Shah, A. Mitchell, M. Klemm, M. Bhaskaran, S. Sriram, and C. Fumeaux, “Efficiency and scalability of dielectric resonator antennas at optical frequencies,” *IEEE Photon. J.* 6, 1–10 (2014).
9. L. Zou, W. Withayachumnankul, C. M. Shah, A. Mitchell, M.

Bhaskaran, S. Sriram, and C. Fumeaux, “Dielectric resonator nanoantennas at visible frequencies,” *Opt. Express* 21, 1344–1352 (2013).

10. A. Petosa, *Dielectric Resonator Antenna Handbook* (Artech House Publishers, 2007).

11. I. Staude, A. E. Miroshnichenko, M. Decker, N. T. Fofang, S. Liu, E. Gonzales, J. Dominguez, T. S. Luk, D. N. Neshev, I. Brener, and Y. Kivshar, “Tailoring directional scattering through magnetic and electric resonances in subwavelength silicon nanodisks,” *ACS Nano* 7, 7824–7832 (2013).

12. F. Wang, Q.-H. Wei, and H. Htoon, “Generation of steep phase anisotropy with zero-backscattering by arrays of coupled dielectric nano-resonators,” *Appl. Phys. Lett.* 105, 121112 (2014).

13. Q.-T. Li, F. Dong, B. Wang, F. Gan, J. Chen, Z. Song, L. Xu, W. Chu, Y.-F. Xiao, Q. Gong, and Y. Li,

“Polarizationindependent and high-efficiency dielectric metasurfaces for visible light,” *Opt. Express* 24, 16309–16319 (2016)

AUTHOR’S PROFILE:



SAPAVAT DEEPA

Received the B.Tech degree in Electronics & Communication Engineering from Sree Dattha Institute of Engineering & Science 2013 from JNTU, Hyderabad, Telangana, India and She completed M.Tech in Electronics & Communication Engineering as specialization in the Department of Electronics & Communication Engineering in 2017 from JNTU Hyderabad Teangana India. She is currently an Assistant Professor with the Department Electronics & Communication Engineering. at SLC College Jntu University, Hyderabad, Telangana India. Her research interests include in the area of RF and Microwave Engineering and Optical networks.

E-mail id: deepaachowan@gmail.com